Canadian Geotechnical Journal

Article

A new mathematical model for the estimation of shear modulus for unsaturated compacted soils

Qian Zhai[a], **Ruize Zhang**[a], **Harianto Rahardjo**[b], **Alfrendo Satyanaga**[c], **Guoliang Dai**[a], **Weimin Gong**[a], **Xueliang Zhao**[a], **and Yuan Shen Chua**[d]

[a]Key Laboratory of Concrete and Prestressed Concrete Structures of Ministry of Education, School of Civil Engineering, Southeast University, Nanjing, 210096 China; [b]School of Civil and Environmental Engineering, Nanyang Technological University, Block N1, Nanyang Ave., Singapore 639798, Singapore; [c]Department of Civil and Environmental Engineering, School of Engineering and Digital Sciences, Nazarbayev University, Kabanbay Batyr Ave., 53, Nur-Sultan 010000, Kazakhstan; [d]Hocklim Engineering Pte Ltd, Singapore

Corresponding author: **Qian Zhai** (email: zhaiqian@seu.edu.cn)

Abstract

Small-strain shear modulus (G) is an essential parameter for many geotechnical analyses. Most of shallow foundations are constructed in an unsaturated soil and the shear modulus of the unsaturated soil fluctuates because of the precipitation, evaporation, and rising of ground water table. In this paper, a new mathematical model is proposed for the estimation of the shear modulus function, G_{unsat}, which defines the relationship between small-strain modulus of unsaturated soil and matric suction. In the proposed model, the soil-water characteristic curve in the form of the degree of saturation is used as the input information. There are additional two parameters named n and C, which can be calibrated with the experimental data, are adopted in the proposed model. The estimated results show good agreement with the experimental data from literature. The proposed method can be used to track the tendency of G_{unsat} and minimize the data points from the laboratory tests.

Key words: shear modulus of saturated soil, soil-water characteristic curve, shear modulus of unsaturated soil, estimation, mathematical model

1. Introduction

The small-strain shear modulus (G) of the geological material is a vital parameter for the estimation of the deformation of a compacted subgrade under dynamic load (Richart et al. 1970; Jardine et al. 1986; Burland 1989). Sawangsuriya (2006) and Zhou (2014) indicated that the shear modulus of soil is commonly within the linear elastic zone corresponding to the strain of less than 0.01%.

Suprunenko (2015) indicated that the shear modulus of a soil is correlated to void ratio, confining pressure, and stress history of soil under fully saturated or dry state conditions. By considering those factors, several well-established models (Hardin and Black 1968; Shibata and Soelarno 1975; Iwasaki and Tatsuoka 1977; Hardin 1978; Shibuya and Tanaka 1996) have been proposed for the estimation of the small-strain shear modulus of soils. Recently, the effect of water content on the shear modulus of a compacted subgrade has captured the attentions of the geotechnical engineers. It has been observed that shear modulus of soil can be affected by the infiltration, evaporation, and fluctuation of water table. Wu et al. (1984) carried out a series of resonant column tests (RCTs) on various types of sands and silts to examine the effect of water content on G. It is observed that G increased with a decrease in water content within a certain range and it decreased when the water content decreases beyond certain value. Qian et al. (1993) also conducted a series of RCTs on various angular sands and produced similar observations. On the other hand, Marinho et al. (1995) conducted a similar test on Cambridge clay and he observed that its shear modulus constantly increased with the increase in soil suction. The rate of increase in shear modulus is gradually reducing with the increase in soil suction. Picornell and Nazarian (1998) conducted experiments on silts and clays and obtained similar observations to Marinho et al. 's (1995) results. Ng et al. (2009) carried out a set of experiments to examine the effect of wetting–drying on G, and they found that the shear modulus functions (SMFs) of unsaturated soil in the drying processes were less than those in the wetting processes. Similar results were gained by Khosravi and McCartney (2012). In addition, Ng and Xu (2012) did the investigation on the effect of the current suction ratio (CSR) and found that G increased with the growth in the CSR. Oh and Vanapalli (2014) summarized the experimental results from several published literatures and indicated that the SMF of the cohesionless soil commonly exhib-

Fig. 1. Typical behaviors of small-strain shear modulus with respect to suction (Oh and Vanapalli 2014).

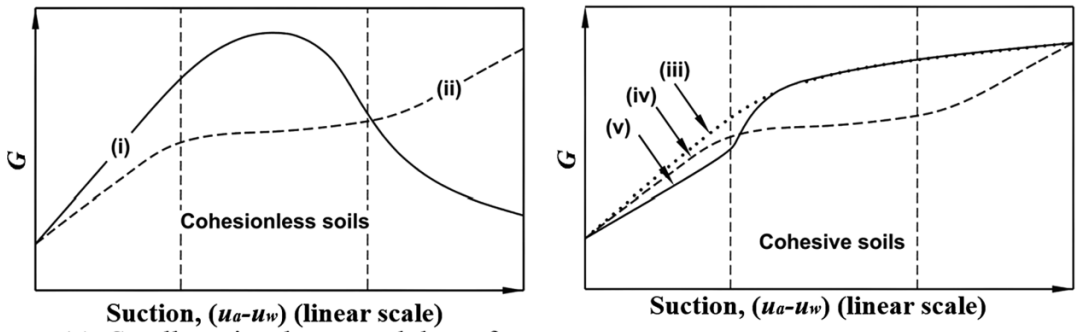

(a) Small-strain shear modulus of cohesionless soils

(b) Small-strain shear modulus of cohesive soils

ited two types of shapes and the cohesive soil commonly behaved three types of shapes as illustrated in Fig. 1. Various researchers (such as Ng and Yung 2008; Biglari et al. 2011; Lu and Kaya 2014; Han and Vanapalli 2016; Ngoc et al. 2019; and Sawangsuriya et al. 2009) have proposed different models for the estimation of the shear modulus from soil suction or water content. However, these models were proposed more empirically rather than theoretically. It is also observed that one model may not have consistently good fitting performance for the experimental data from different published literature.

In this paper, a new mathematical model was derived for the estimation of the shear modulus for unsaturated soil. In the derivation, the pores in unsaturated soil are divided into two groups including (i) wet pores that are fully filled with water and (ii) dry pores from which water has fully drained out. In the proposed models, the soil-water characteristic curve (SWCC) in the form of the degree of saturation (*S*-SWCC) was employed. The incompressibility of the pores with diameter less than 100 nm is also considered. The model parameters are determined by best fitting the proposed model with the experimental data. It is observed that the proposed model has good performance in describing the behaviors of shear modulus of unsaturated soil as compared with experimental data from literature.

2. Existing models for the shear modulus of soils

Different models for the estimation of the shear modulus of soils were reviewed in this section. The theories adopted in these models were used as the basis in the derivation of the proposed model.

2.1. Models for *G* of saturated or dry soils

The work from Sawangsuriya (2006) indicated that shear modulus was mainly governed by three factors, including (i) the normal stresses or the confining pressure (σ_0') exerted on the soil, (ii) the overconsolidation ratio (OCR), and (iii) the void ratio (e) or the density of the soil (ρ). As a result, Sawangsuriya (2006) proposed a general equation for the estimation of the shear modulus as illustrated in eq. 1.

$$(1) \quad G = A(\mathrm{OCR})^k f(e) P_a^{(1-n)} (\sigma_n)^n$$

where A, k, and n are fitting parameters; OCR is the overconsolidation ratio; $f(e)$ is the original void ratio function; P_a is the atmospheric pressure; and σ_n is the effective normal stress.

2.2. Mathematical models for the SMF

Oloo (1998) proposed the model for the estimation of the resilient modulus from the matric suction. The model from Oloo (1998) has a similar form as eq. 1. Vanapalli et al. (1996) proposed the model for the estimation of shear strain behavior for the unsaturated soil. Sawangsuriya et al. (2009) proposed eq. 2 to compute the G_{unsat} of unsaturated compacted soils from soil suction.

$$(2) \quad G_{unsat} = A f(e) (\sigma_n)^n + C\psi\Theta^\kappa$$

where A, C, and κ are fitting parameters; n is the stress exponent ($n = 0.5$ is recommended by Sawangsuriya et al. (2009)); Θ is the normalized volumetric water content that can be obtained by SWCC; $f(e)$ is the void ratio function; σ_n is the net normal stress; and ψ is the matric suction.

By adopting the concept of modified effective stress from Bishop (1959), eq. 2 can be modified to eq. 3 as follows:

$$(3) \quad G_{unsat} = A f(e) [\sigma_n + \psi\Theta^\kappa]^n$$

where A, n, and κ are fitting parameters; others are the same as those in eq. 2.

Considering the effect of degree of saturation on the shear modulus, Lu and Kaya (2014) proposed a single-parameter empirical equation as follows:

$$(4) \quad \frac{G_{unsat} - G_{dry}}{G_{sat} - G_{dry}} = \left(\frac{\theta - \theta_{dry}}{\theta_{sat} - \theta_{dry}}\right)^m$$

where m is a fitting parameter; G_{sat} is the small-strain shear modulus for the fully saturated soil; G_{dry} is the small-strain shear modulus for the dry soil; G_{unsat} is the small-strain shear

Fig. 2. Schematic diagrams of the proposed states.

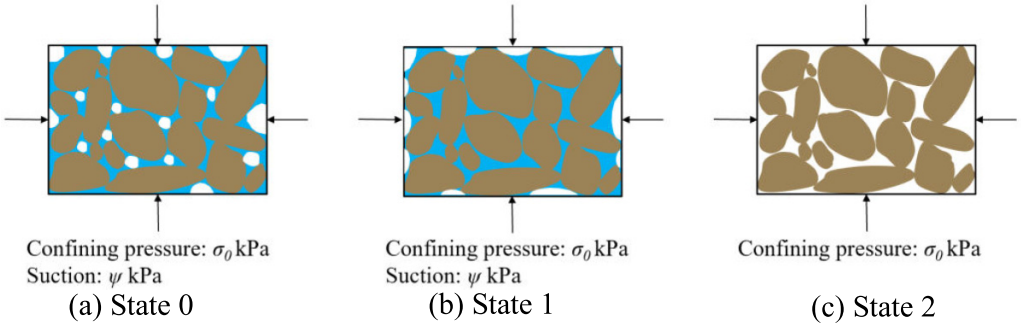

modulus for the unsaturated soil; θ is volumetric water content for the unsaturated soil; θ_{sat} is the saturated volumetric water content; and θ_{dry} is the volumetric water content for the dry soil.

By introducing the reference point, Han and Vanapalli (2016) improved eq. 2 into eq. 5 as follows:

$$(5) \qquad \frac{G_{unsat} - G_{sat}}{G_{ref} - G_{sat}} = \frac{\psi}{\psi_{ref}}\left(\frac{S}{S_{ref}}\right)^{\xi}$$

where ξ is a fitting parameter; G_{sat} is the small-strain shear modulus for the saturated soil; G_{ref} is the small-strain shear modulus corresponding to the reference state; ψ is the matric suction; ψ_{ref} is the matric suction corresponding to the reference state; S is the degree of saturation; and S_{ref} is the degree of saturation corresponding to the reference state.

3. Theory

The derivations of the proposed model for the estimation of the shear modulus of unsaturated soil are explained in this section. The assumptions adopted in the derivations are also clearly introduced.

3.1. Assumptions adopted in the derivation

There are seven major assumptions adopted in the derivations, which are (i) the deformation of a soil results purely from the deformation of the pores (both the soil particles and water phase is incompressible); (ii) the small-strain moduli of an unsaturated soil (including shear modulus, Young's modulus, and bulk modulus) are defined as the slope on the corresponding stress–strain curve under constant suction; (iii) the Poisson's ratio is assumed to be constant for the entire suction range; (iv) the pores in unsaturated soil could be represented by a series of simplified fractions, which could be categorized into either the fraction with wet pores (fully filled with water) or fraction with the dry pores; (v) the soil sample of either saturated soil or unsaturated soil is uniform and the void ratio of the fraction is consistent with that of the soil sample; (vi) the deformation of the dry and wet pores in a soil is proportional to their original volumes; and (vii) the pore size distribution of a compacted soil remains constant when suction varies. It is known that water drains out of the pores in soil following the Kelvin's law, which means that water drains out from the large pores first and progressively from the smaller pores. In this case, the dry proportion of unsaturated soil contains most of large pores, while the wet proportion contains most of small pores. Arya and Paris (1981) proposed the fraction method, which assumes all the fraction to have the same porosity, to estimate the SWCC from the grain size distribution data. Even though each fraction has the same porosity in Arya and Paris (1981)'s fraction model, the amount of the pores with different sizes can be different and can be defined by the pore size distribution function. Arya and Paris (1981)'s assumption has been adopted by Satyanaga et al. (2017) and Zhai et al. (2020*a*). In this paper, Arya and Paris (1981)'s assumption was also adopted in the proposed method.

In the proposed model, three different states, such as State 0, State 1, and State 2, are considered. State 0 defines the state of unsaturated condition under both net confining stress of σ_0 kPa and matric suction of ψ kPa; State 1 defines the saturated state under both confining stress of σ_0 kPa and suction of ψ kPa; State 2 defines the state of the completely dried condition under only net confining stress of σ_0 kPa. The schematic diagrams of those three states are illustrated in Fig. 2.

3.2. Derivation of the model

The small-strain bulk modulus of the soil is commonly defined by eq. 6 as follows:

$$(6) \qquad K = -\frac{dp}{dV/V}$$

where K is the small-strain bulk modulus, p is the applied stress, V is the volume of soil, and dV is the variation of soil volume.

Note that both small-strain bulk modulus and small-strain shear modulus are related to the small-strain Young's modulus as shown in eqs. 7 and 8.

$$(7) \qquad K = \frac{E}{3(1-2\nu)}$$

$$(8) \qquad G = \frac{E}{2(1+\nu)}$$

Fig. 3. Schematic diagrams of the relationship of wet pores, dry pores, compressible pores, and incompressible pores.

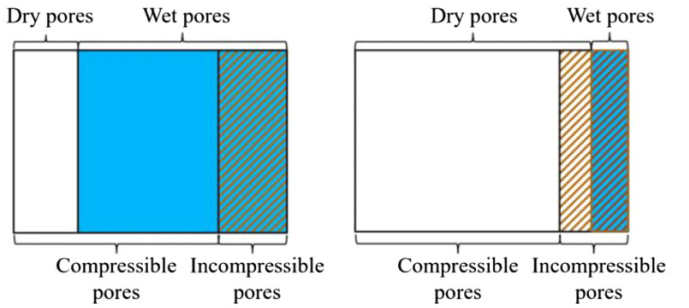

(a) scenario with low suction (b) scenario with high suction

Fig. 4. Pore size cumulative curve converted from soil-water characteristic curve.

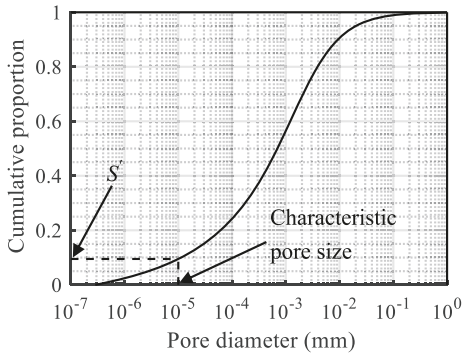

Fig. 5. The typical soil-water characteristic curve adopted for the demonstration.

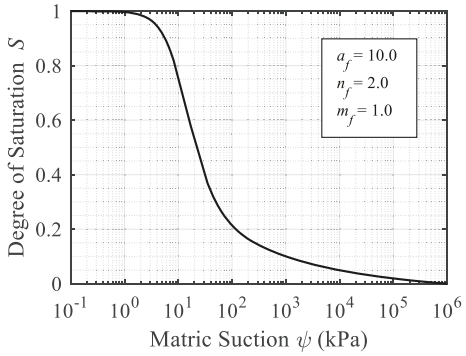

where E is the small-strain Young's modulus; G is the small-strain shear modulus, and v is the Poisson's ratio.

Substituting eqs. 7 and 8 into eq. 6 gives eq. 9 as follows:

$$\frac{\mathrm{d}V}{\mathrm{d}p} = -C_0\frac{V}{G} \tag{9}$$

where C_0 equals to $\frac{3(1-2v)}{2(v+1)}$, if v is a constant based on the assumption (iii), then the coefficient C_0 is also a constant.

This equation relates the small-strain shear modulus to the volume change of a soil. Based on assumption (iv), the pores in the unsaturated soil could be represented by a series of wet pores and dry pores. Thus, the volume change of the soil, which is equal to the total volume change of pores, can be divided into two parts, i.e., the volume change of wet pores ($\mathrm{d}V_\mathrm{w}$) and volume change of dry pores ($\mathrm{d}V_\mathrm{d}$). As a result, the total volume change with respect to load can be expressed in eq. 10 as follows:

$$\frac{\mathrm{d}V}{\mathrm{d}p} = \frac{\mathrm{d}V_\mathrm{w}}{\mathrm{d}p} + \frac{\mathrm{d}V_\mathrm{d}}{\mathrm{d}p} \tag{10}$$

where V denotes the total pore volume, V_w denotes the volume of wet pores, and V_d denotes the volume of dry pores.

To calculate $\mathrm{d}V_\mathrm{w}/\mathrm{d}p$ and $\mathrm{d}V_\mathrm{d}/\mathrm{d}p$ in an unsaturated soil, three identical soil samples in State 0, State 1, and State 2, respectively, are considered. The soil sample illustrated in State 0 soil is divided into two types of fractions such as the fractions containing only wet pores and fractions containing only dry pores. As the soil sample is uniform, both types of fractions should have a consistent void ratio, which is same as that for the soil sample shown in State 0. Assuming the meniscus exists at external rim of the fractions with wet pores, those fractions can keep saturated and are subjected to both confining pressure of σ_0 kPa and the suction stress of ψ kPa. On the other hand, there is no meniscus in the fractions with dry pores and the fraction is only subjected to confining pressure of σ_0 kPa. As a result, eqs. 11 and 12 can be obtained as follows:

$$\left.\frac{\mathrm{d}V_\mathrm{w}}{\mathrm{d}p}\right|_{\text{State 0}} = \left.\frac{\mathrm{d}V_\mathrm{w}}{\mathrm{d}p}\right|_{\text{State 1}} = \frac{\mathrm{d}V_1}{\mathrm{d}p}\cdot\frac{V_\mathrm{w}}{V_{\mathrm{p}1}} \tag{11}$$

$$\left.\frac{\mathrm{d}V_\mathrm{d}}{\mathrm{d}p}\right|_{\text{State 0}} = \left.\frac{\mathrm{d}V_\mathrm{d}}{\mathrm{d}p}\right|_{\text{State 2}} = \frac{\mathrm{d}V_2}{\mathrm{d}p}\cdot\frac{V_\mathrm{d}}{V_{\mathrm{p}2}} \tag{12}$$

where $\mathrm{d}V_1$ is the change in the volume of the soil in State 1 under a given stress increment; $V_{\mathrm{p}1}$ is the total volume of the pores in the soil in State 1; $\mathrm{d}V_2$ is the change in the volume of the soil in State 2 under a given stress increment; and $V_{\mathrm{p}2}$ is the total volume of the pores in the soil in State 2.

Noting that the relationship between the degree of saturation (S) and V_w, as well as that between the volume of pores and void ratio, eqs. 11 and 12 can be rearranged as eqs. 13 and 14, respectively:

$$\left.\frac{\mathrm{d}V_\mathrm{w}}{\mathrm{d}p}\right|_{\text{State 1}} = \frac{\mathrm{d}V_1}{\mathrm{d}p}\cdot S\cdot\frac{V_{\mathrm{p}0}}{V_{\mathrm{p}1}} = \frac{\mathrm{d}V_1}{\mathrm{d}p}\cdot S\cdot\frac{e_0}{e_1} = \frac{\mathrm{d}V_1}{\mathrm{d}p}\cdot S \tag{13}$$

$$\left.\frac{\mathrm{d}V_\mathrm{d}}{\mathrm{d}p}\right|_{\text{State 2}} = \frac{\mathrm{d}V_2}{\mathrm{d}p}\cdot(1-S)\cdot\frac{V_{\mathrm{p}0}}{V_{\mathrm{p}2}} = \frac{\mathrm{d}V_2}{\mathrm{d}p}\cdot(1-S)\cdot\frac{e_0}{e_2} = \frac{\mathrm{d}V_2}{\mathrm{d}p}\cdot(1-S) \tag{14}$$

where S is the degree of saturation under a given suction, $V_{\mathrm{p}0}$ is the total volume of the pores in the soil in State 0; e_0 is the void ratio of the State 0 soil; e_1 is the void ratio of the State 1 soil; e_2 is the void ratio of the State 2 soil; and others are the same as those in eqs. 11 and 12.

Fig. 6. The schematic illustration of the implications of the parameters.

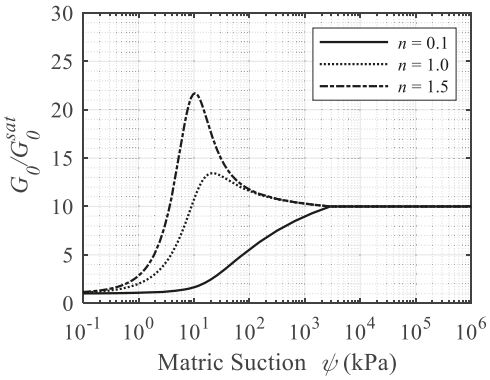

(a) The effect of n

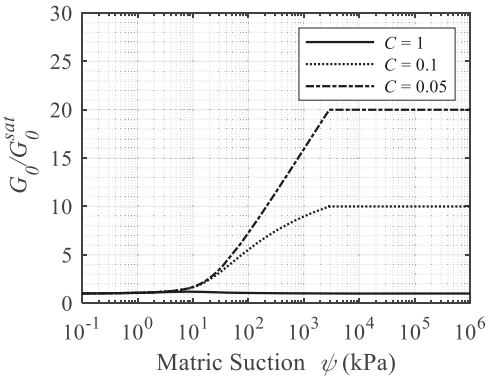

(b) The effect of C

Substituting eqs. 13, 14, and 10 into eq. 9 gives eq. 15 as follows:

$$(15)\quad G_{unsat} = C_0 \frac{V_0}{C_0 \frac{V_1}{G_1}\cdot S + C_0 \frac{V_2}{G_2}\cdot (1-S)} = \frac{1}{\frac{1}{G_1}\cdot S\cdot \frac{V_1}{V_0} + \frac{1}{G_2}\cdot (1-S)\cdot \frac{V_2}{V_0}} = \frac{1}{\frac{1}{G_1}\cdot S\cdot \frac{e_1+1}{e_0+1} + \frac{1}{G_2}\cdot (1-S)\cdot \frac{e_2+1}{e_0+1}} = \frac{1}{\frac{1}{G_1}\cdot S + \frac{1}{G_{dry}}\cdot (1-S)}$$

where V_0 is the volume of the soil in State 0; G_{unsat} is the small-strain shear modulus of the soil in State 0 or unsaturated state; G_1 is the small-strain shear modulus of the soil in State 1; G_2 is the small-strain shear modulus of the soil in State 2 and is equal to the small-strain shear modulus of dry soil sample G_{dry}; and others are the same as those in eqs. 13 and 14.

As the parameters of k, OCR, and $f(e)$ are commonly constant, eq. 1 can be simplified as eq. 16 as follows:

$$(16)\quad G = A(P_a)^{1-n}(\sigma_n)^n$$

where A and n are fitting parameters; P_a is the atmospheric pressure; and σ_n is the confining net pressure.

The soil fraction in State 1 is surrounded by contractile skins and subjected to suction stress of ψ kPa. The G_1 can be calculated from eq. 17 as follows:

$$(17)\quad G_1 = A(P_a)^{1-n}(\sigma_0 + \psi)^n$$

where ψ is the matric suction.

Substituting eq. 17 into eq. 15, the following equation can be obtained:

$$(18)\quad G_{unsat} = \frac{1}{\frac{1}{A(P_a)^{1-n}(\sigma_0+\psi)^n}\cdot S + \frac{1}{G_{dry}}\cdot (1-S)}$$

A is a fitting parameter that can be determined by the measured G_{unsat} data at a given suction; thus, an attempt to eliminate it was made. As the unsaturated soil properties are commonly referred to the corresponding saturated properties, the G_{sat} at zero suction was selected. Considering the relationship between A and G_{sat} defined by eq. 16, and rearranging it gives eq. 19 as follows:

$$(19)\quad A = \frac{G_{sat}}{(P_a)^{1-n}(\sigma_0)^n}$$

Substituting it into eq. 18, the unsaturated shear modulus can be estimated from the saturated shear modulus by eq. 20 as follows:

$$(20)\quad G_{unsat} = G_{sat}\frac{\left(1+\frac{\psi}{\sigma_0}\right)^n}{S + \frac{G_{sat}}{G_{dry}}\cdot (1-S)\cdot \left(1+\frac{\psi}{\sigma_0}\right)^n}$$

It is noted that G_{sat} and G_{dry} are commonly constant regardless the variation of soil suction. Equation 20 can then be simplified as eq. 21 by introducing a new coefficient C as follows:

$$(21)\quad G_{unsat} = G_{sat}\frac{\left(1+\frac{\psi}{\sigma_0}\right)^n}{S + C\cdot (1-S)\cdot \left(1+\frac{\psi}{\sigma_0}\right)^n}$$

where

$$(22)\quad C = \frac{G_{sat}}{G_{dry}}$$

3.3. Consideration of incompressible pores

A great number of studies have shown that the pores within a cohesive soil can be divided into two groups, i.e., intra-aggregate pores and inter-aggregate pores. The pore size distribution curve segment corresponding to the intra-aggregate pores remains constant while loading or changing the water content (Delage et al. 1996; Lloret et al. 2003; Romero and Simms 2008; Monroy et al. 2010; Kuila and Prasad 2013; Otálvaro et al. 2015). In addition, the current literature data showed that the characteristic pore size (the maximum diameter) corresponding to the intra-aggregate pores range from 10^{-6} to 10^{-4} mm. For the cohesionless soils, it has been observed that under the stress range without disintegration, the segment at the most left of the curve remains unchanged (Juang and Lovell 1986; Kutílek et al. 2006). In this study, these pores are referred to as minimal pores. In other words, the number and size of pores corresponding to this curve section could also be considered constant. The maximum pore diameter of this segment typically ranges from 10^{-3} to 10^{-1} mm (Minagawa et al. 2008; Stingaciu et al. 2010; Wang et al. 2023). Therefore, the pores in a soil can be divided into two parts—compressible pores and incompressible pores. The number and size of incompressible pores remain

Table 1. Basic information about cohesive soil samples.

Soils	Classification[c]	Liquid limit	Plastic index	Optimum moisture content (%)	Maximum dry unit weight (kN/m)	Porosity	Specific gravity	Pre-consolidation condition	Confining pressure (kPa)
ML-Std-Opt[a]	ML	28	11	13.5	17.9	–	2.69	Compacted	35
CL-2-Std-Opt[a]	CL	26	9	16	17.7	–	2.66	Compacted	35
CL-1-Std-Opt[a]	CL	42	24	22	15.8	–	2.69	Compacted	35
CH-Std-Opt[a]	CH	85	52	27.5	14.4	–	2.75	Compacted	35
Bonny silt[b]	ML	–	–	–	–	0.46	–	Compacted	0[d]
Hopi silt[b]	SC	–	–	–	–	0.44	–	Compacted	0[d]
Iowa silt[b]	ML	–	–	–	–	0.49	–	Compacted	0[d]
Claystone[b]	CL	–	–	–	–	0.51	–	Compacted	0[d]
Bentonite[b]	CH	–	–	–	–	0.69	–	Compacted	0[d]
Missouri clay[b]	CL	–	–	–	–	0.41	–	Compacted	0[d]

[a]Datasets retrieved from Sawangsuriya et al. (2009).
[b]Datasets retrieved from Dong and Lu (2016).
[c]The soil samples are classified by the Unified Soil Classification System. No relevant data are provided in the literature.
[d]The confining pressure reported in the original study is 0 kPa, and 0.01 kPa is adopted in the proposed model.

Table 2. Basic information about cohesionless soil samples.

Soils	USCS Soil Classification	Porosity	Specific gravity	Mean particle size (mm)	Coefficient of uniformity	Pre-consolidation condition	Confining pressure (kPa)
Sand 1[a]	SP	0.42	2.65	0.19	1.29	Deposited with constant free-fall height	24
Sand 2[a]	SP	0.42	2.65	0.19	1.29	Deposited with constant free-fall height	70
Sand 3[a]	SP	0.42	2.65	0.19	1.29	Deposited with constant free-fall height	100
Sand 4[a]	SP	0.42	2.65	0.19	2.50	Deposited with constant free-fall height	70
Sand 5[a]	SP	0.42	2.65	0.27	1.29	Deposited with constant free-fall height	70

[a]Datasets retrieved from Khosravi et al. (2018) and Sand 1, 2, and 3 are the same soils under different confining pressures.

Table 3. Fitting parameters of soil-water characteristic curve (SWCC).

Soils		SWCC fitting parameters			SWCC variables	
		a_f (kPa)	n_f	m_f	AEV (kPa)	ψ_r (kPa)
ML-Std-Opt	Cohesive soils	40.65	1.65	0.55	21.32	327.87
CL-2-Std-Opt		207.87	0.89	0.50	90.36	2364.00
CL-1-Std-Opt		235.43	0.82	0.57	91.85	2490.32
CH-Std-Opt		1208.40	0.91	0.74	310.71	3087.12
Bonny silt		12.67	1.31	1.03	4.57	127.00
Hopi silt		16.71	2.48	0.57	10.81	86.45
Iowa silt		11.06	1.70	0.71	5.58	90.27
Claystone		66.49	1.84	0.47	38.18	451.67
Bentonite		42.79	2.79	0.23	31.33	150.79
Missouri clay		36.87	1.65	0.52	19.59	300.98
Sand 1	Cohesionless soils	3.87	55.41	0.43	3.80	4.42
Sand 2		4.67	10.44	0.85	4.14	7.27
Sand 3		5.75	60.00	0.51	5.76	6.28
Sand 4		4.77	7.03	0.87	3.99	8.95
Sand 5		3.35	7.67	0.93	2.83	5.86

Fig. 7. Best fitted soil-water characteristic curves (SWCCs) for the cohesive soils.

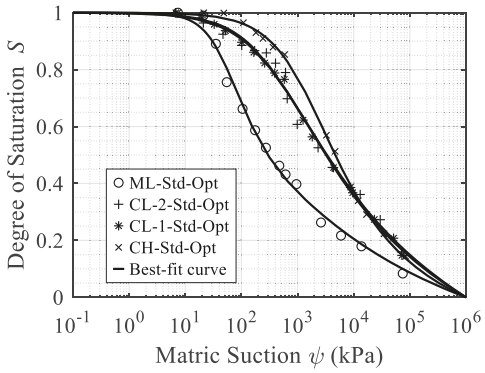

(a) Best fitted SWCCs of soils redrawn from Sawangsuriya et al.

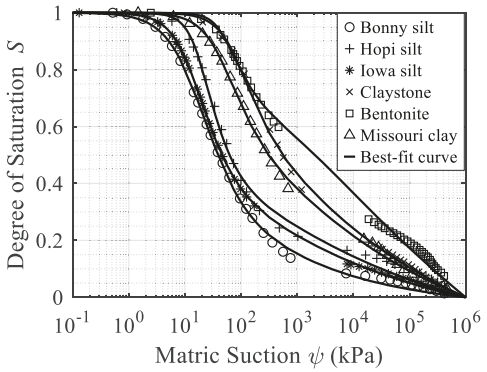

(b) Best fitted SWCCs of soils redrawn from Dong and Lu (2016)

Fig. 8. The best fitted soil-water characteristic curves for the sandy soils redrawn from Khosravi et al. (2018).

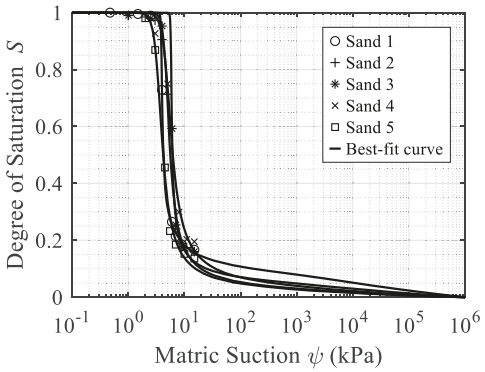

constant with the change of stress and suction. Also, its number and size are the same among State 0, 1, and 2. Considering the presence of incompressible pores, eqs. 11 and 12 should be corrected as the following eqs. 23 and 24:

$$(23)\quad \left.\frac{dV_w}{dp}\right|_{State\,0} = \left.\frac{dV_w}{dp}\right|_{State\,1} = \frac{dV_1}{dp}\cdot\frac{V_w^c}{V_{p1}^c}$$

$$(24)\quad \left.\frac{dV_d}{dp}\right|_{State\,0} = \left.\frac{dV_d}{dp}\right|_{State\,2} = \frac{dV_2}{dp}\cdot\frac{V_d^c}{V_{p2}^c}$$

where V_w^c is the volume of compressible pores in the wet part of State 0 soil; V_d^c is the volume of compressible pores in the dry part of State 0 soil; V_{p1}^c is the volume of compressible pores in the State 1 soil; V_{p2}^c is the volume of compressible pores in the State 2 soil; and others are the same as those in eqs. 11 and 12.

To calculate V_w^c/V_{p1}^c and V_d^c/V_{p2}^c, the relationship of wet pores, dry pores, compressible pores, and incompressible pores, as illustrated in Fig. 3, should be articulated. According

Fig. 9. The measured data of small-strain shear modulus of the cohesive soils.

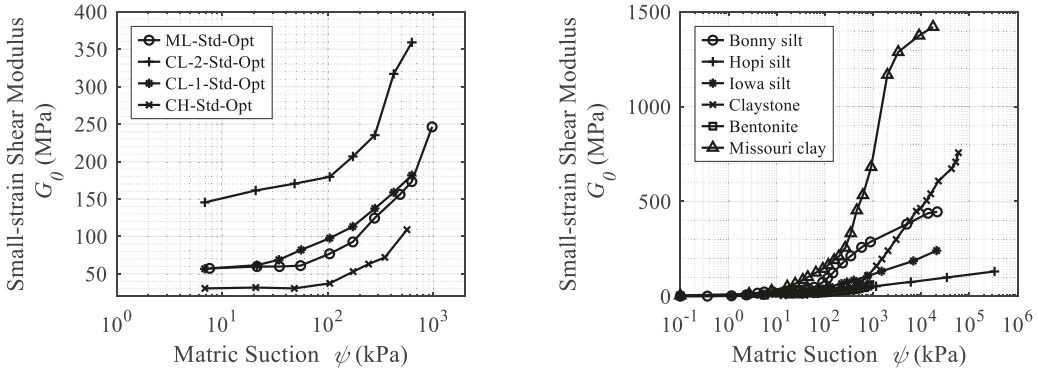

(a) Measured small-strain shear modulus data redrawn from Sawangsuriya et al.

(b) Measured small-strain shear modulus data redrawn from Dong and Lu (2016)

Fig. 10. The measured data of small-strain shear modulus of sandy soils redrawn from Khosravi et al. (2018).

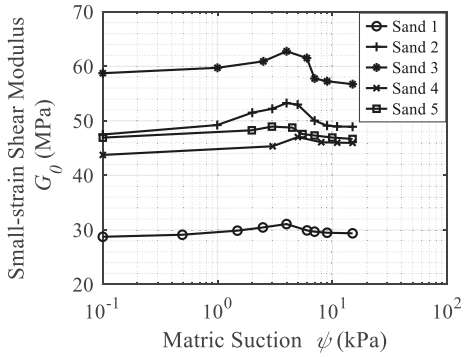

to whether incompressible pores saturate or not, there are two scenarios, i.e., scenario 1 and 2. Scenario 1 refers to the situation when the incompressible pores are fully saturated, while scenario 2 refers to the situation when the incompressible pores are partially saturated. For scenario 1, V_c^d/V_{p2}^c can be calculated as the following eqs. 25 and 26:

$$(25)\quad \frac{V_w^c}{V_{p1}^c} = \frac{V_w - V_p^i}{V_{p1} - V_p^i} = \frac{V_w/V_{p0} - V_p^i/V_{p0}}{V_{p1}/V_{p0} - V_p^i/V_{p0}} = \frac{S - S'}{e_1/e_0 - S'} = \frac{S - S'}{1 - S'}$$

$$(26)\quad \frac{V_d^c}{V_{p2}^c} = \frac{V_{p2} - V_w}{V_{p2} - V_p^i} = \frac{V_{p2}/V_{p0} - V_w/V_{p0}}{V_{p2}/V_{p0} - V_p^i/V_{p0}} = \frac{1 - S}{e_2/e_0 - S'} = \frac{1 - S}{1 - S'} = 1 - \frac{S - S'}{1 - S'} = 1 - \frac{V_w^c}{V_{p1}^c}$$

where V_p^i is the volume of incompressible pores and S' is the incompressible proportion of the volume of pores.

For scenario 2, the V_w^c/V_{p1}^c is equal to zero, and V_d^c/V_{p2}^c is equal to 1. To combine these two scenarios, S_e is used to denote V_w^c/V_{p1}^c, and therefore V_d^c/V_{p2}^c is equal to $1-S_e$.

According to Zhai and Rahardjo (2015), by converting suction into pore size with eq. 27, SWCC in the form of degree of saturation can be treated as the pore cumulative curve as illustrated in Fig. 4. In this diagram, the value on the curve corresponding to the maximum size of the incompressible pore (characteristic pore size) is S'. In this way, the value of S' of cohesive and cohesionless soils can be determined, and S_e can be calculated using eq. 28

$$(27)\quad \psi = \frac{4T\cos\alpha}{d}$$

where T is the surface tension of water, and is 0.072 N/m at 25° C; α is the contact angle of soil; and d is the diameter of the pore.

Zhai et al. (2019, 2020*b*) indicated that hydroscopic water is dominated in the cohesive soil when the soil suction was greater than 3100 kPa. In a cohesive soil, pores with size less than equivalent suction of 3100 kPa can be treated as intra-aggregate pores. As a result, Zhai et al. (2019) proposed to modify the conventional SWCC by replacing S with S_e as defined in eq. 28 by removal of hydroscopic water in soil. This modified SWCC is also adopted in this paper to remove the effect of incompressible pores on the SMF.

$$(28)\quad S_e = \begin{cases} \dfrac{S - S'}{1 - S'} & (S > S') \\ 0 & (S \le S') \end{cases}$$

where S' is the soil suction corresponding to 3100 kPa for cohesive soil, and residual degree of saturation for cohesionless soil.

Therefore, eq. 21 can be rewritten into eq. 29:

$$(29)\quad G_{unsat} = G_{sat}\frac{\left(1 + \frac{\psi}{\sigma_0}\right)^n}{S_e + C\cdot(1 - S_e)\cdot\left(1 + \frac{\psi}{\sigma_0}\right)^n}$$

3.4. Illustration of effects of the parameters in the proposed model

To illustrate the effect of parameters in these two equations on the curve, illustration plots are developed below. For illustration purposes, σ_0 is set as 1 kPa, and a typical SWCC (Fig. 5) is expressed by using Fredlund and Xing (1994)'s equation, as illustrated in eq. 30, with fitting parameters (a_f =10 kPa,

Fig. 11. The fitting results of the cohesive sample soils redrawn from Sawangsuriya et al. (2009).

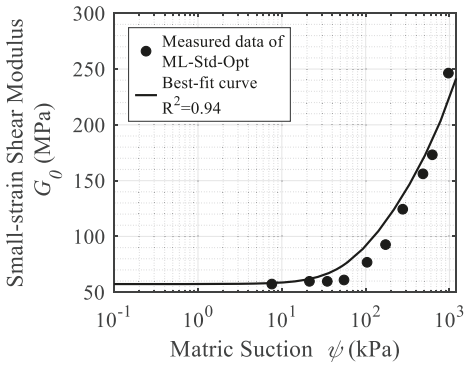

(a) The fitting results of ML-Std-Opt

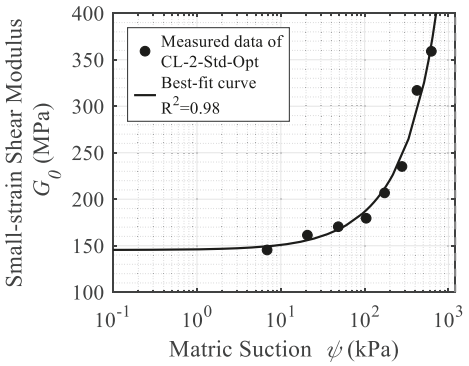

(b) The fitting results of CL-2-Std-Opt

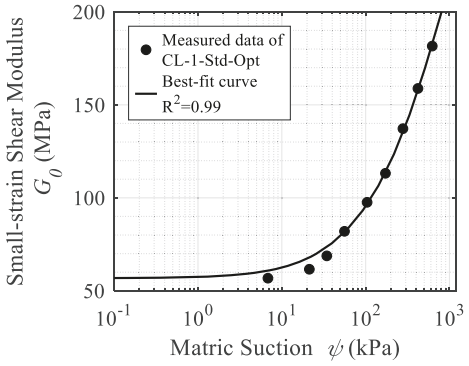

(c) The fitting results of CL-1-Std-Opt

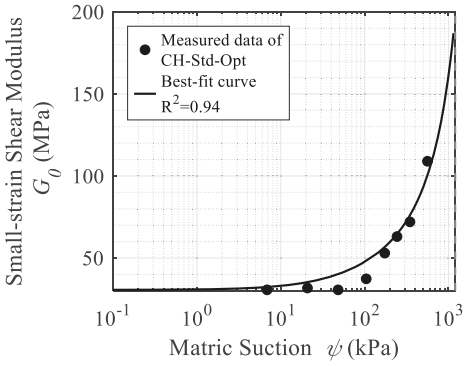

(d) The fitting results of CH-Std-Opt

$n_f = 2$, and $m_f = 1$) is employed.

$$(30)\quad S = C(\psi)\cdot\frac{1}{\left\{\ln\left[e+\left(\frac{\psi}{a_f}\right)^{n_f}\right]\right\}^{m_f}} = \left[1-\frac{\ln\left(1+\frac{\psi}{C_r}\right)}{\ln\left(1+\frac{10^6}{C_r}\right)}\right]\cdot\frac{1}{\left\{\ln\left[e+\left(\frac{\psi}{a_f}\right)^{n_f}\right]\right\}^{m_f}}$$

where ψ is soil suction; a_f, m_f, and n_f are fitting parameters; C_r is an input value for the rough estimation of the residual suction, which is commonly set to 1500 kPa as recommended by Zhai and Rahardjo (2012); and e is Euler's number.

As illustrated in eq. 29, the shear modulus of unsaturated soil is mainly governed by the fitting parameters C and n and the shape of SWCC. By setting C equals to 0.1, the estimated G_{unsat} values from the typical SWCC by adopting n of 0.1, 1, and 1.5 are illustrated in Fig. 6*a*. On the other hand, the estimated G_{unsat} values from the typical SWCC by adopting n equals to 0.1 and C to be equal to 0.01, 0.1, and 1 are illustrated in Fig. 6*b*. As shown in Fig. 6, the shape of the estimated G_{unsat} is mainly controlled by the parameters C and n. It seems the slope is mainly controlled by the parameter C, while the peak point is mainly controlled by the parameter n. A smaller value of C gives a steeper slope of curve, and a larger value of n gives a higher peak point of the curve.

4. Verification of the proposed model

To verify the performance of eq. 29, a total of 15 RCT-based datasets from Sawangsuriya et al. (2009), Dong and Lu (2016), and Khosravi et al. (2018) are adopted. The soil samples are divided into two groups such as sandy soils and cohesive soils. The index properties of the soil samples are illustrated in Tables 1 and 2 for the cohesive soils and the sandy soils, respectively.

The fitting parameters in Fredlund and Xing (1994)'s equation for those soils are illustrated in Table 3 and the best fitted SWCCs and the air entry value (AEV) and the residual suction (ψ_r) are shown in Figs. 7 and 8. The SWCC variables are computed from the fitting parameters following the method proposed by Zhai and Rahardjo (2012) and Zhai et al. (2017) and are also illustrated in Table 3.

The measured data for the small-strain shear modulus with respect to matric suction are illustrated in Figs. 9 and 10 for the cohesive soils and sandy soils, respectively. It is noteworthy that the SWCC and the SMF datasets are all measured during the drying process.

Equation 29 is used to best fit with the measured data as shown in Figs. 9 and 10. Both the coefficient of determination (R^2) and root mean square error (RMSE), which are defined in eqs. 31 and 32, respectively, are computed and illustrated in

Fig. 12. The fitting results of the cohesive sample soils redrawn from Dong and Lu (2016).

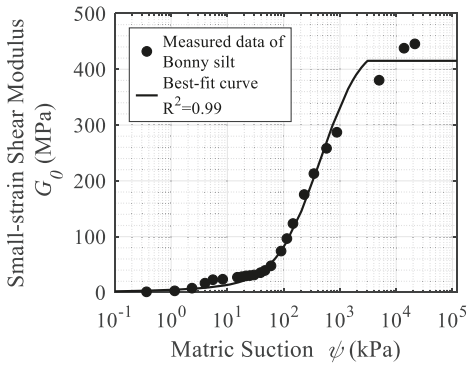

(a) The fitting results of Bonny silt

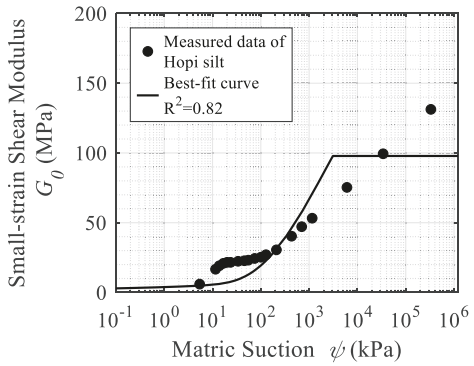

(b) The fitting results of Hopi silt

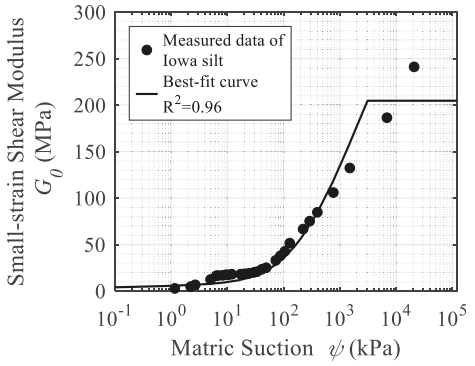

(c) The fitting results of Iowa silt

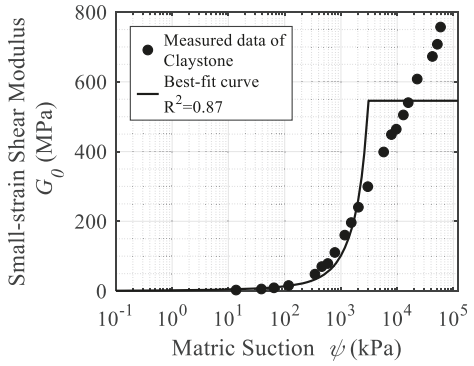

(d) The fitting results of Claystone

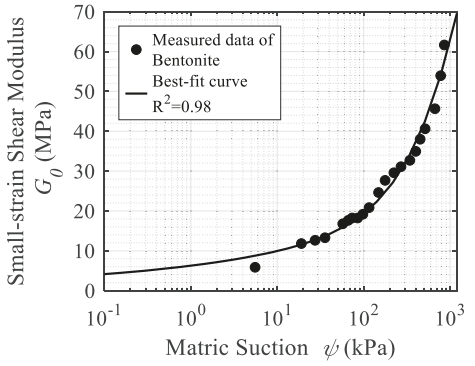

(e) The fitting results of Bentonite

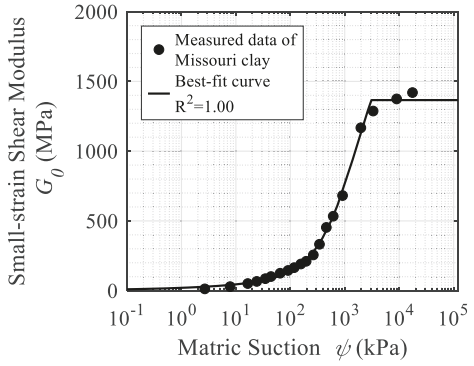

(f) The fitting results of Missouri clay

Table 4. The best fitted results for those cohesive soils and the sandy soils are illustrated in Figs. 11–13.

$$R^2 = 1 - \frac{\mathrm{SSE}}{\mathrm{SST}} \tag{31}$$

$$RMSE = \sqrt{\frac{1}{N} \cdot \mathrm{SSE}} \tag{32}$$

where N is the total number of the data points within a dataset; SSE is the sum of the squared errors as defined in the eq. 27; and SST is the sum of the squares total as defined in eq. 28.

$$\mathrm{SSE} = \sum_{i=1}^{N} (\widehat{y}_i - y_i)^2 \tag{33}$$

where $\widehat{y}_i$ is the predicted value of the dependent variable at the ith data point, and y_i is the value of the dependent variable at the ith data point.

$$\mathrm{SST} = \sum_{i=1}^{N} (y_i - \bar{y})^2 \tag{34}$$

where $\bar{y}$ is the mean value of the dependent variable of all data.

Fig. 13. The fitting results of the sandy soils redrawn from Khosravi et al. (2018).

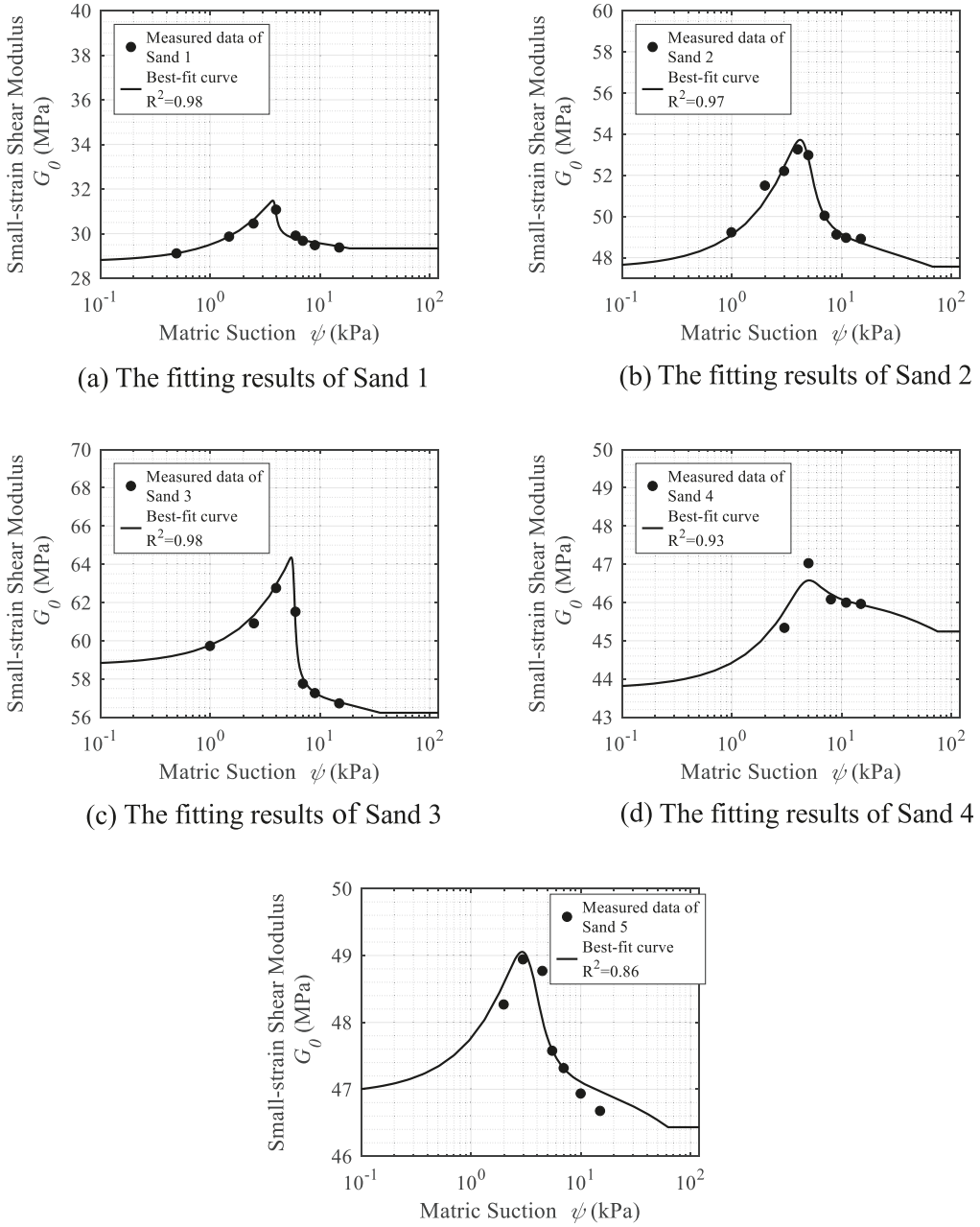

(a) The fitting results of Sand 1

(b) The fitting results of Sand 2

(c) The fitting results of Sand 3

(d) The fitting results of Sand 4

(e) The fitting results of Sand 5

From the plots, it can be shown that overall, this model can capture well the trend of the small-margin shear modulus with changing suction. In addition, the goodness-of-fit indices also underpin this argument. All of the RMSE shown in Table 4 are sufficiently small. Most of R^2 is greater than 0.9, which, according to Witczak et al. (2002), indicates excellent fitting performances. Moreover, this model can represent the curves of cohesive soils slightly better than those of cohesionless ones, and this may imply that although the proposed model can fit data of cohesionless soils satisfactorily, it might be more suitable for cohesive soils.

It is observed that the values of model parameters n and C for the cohesionless soils are higher than those for the cohesive soils. As mentioned in 3.2 Derivation of the model, a larger n implies a higher peak of the curve, while a relatively large C is associated with a steeper slope. The characteristic curves of G_{unsat} for cohesionless soils usually feature a peak value of G_{unsat}. Therefore, they often have a larger n. In addition, the values of G for cohesionless soils with respect to the suction are not as sensitive as cohesive soils. Thus, they might have a larger C. More importantly, the results of best-fit parameters show that the values of C for cohesionless soil are around one, while those for cohesive soils are typically near zero. This reveals that the G_{unsat} of a cohesionless soil in the dry state is approximately equal to that corresponding to the saturated state, while the G_{unsat} of a cohesive soil near the

Table 4. The results of S', fitting parameters, and goodness-of-fit indices of model 1 and 2.

Soils		S'	Best-fit parameters		Goodness-of-fit indices	
			n	C	R^2	RMSE
ML-Std-Opt	Cohesive soils	0.282	0.000	0.152	0.94	14.23
CL-2-Std-Opt		0.510	0.040	1×10^{-4}	0.98	10.36
CL-1-Std-Opt		0.505	0.280	0.206	0.99	3.12
CH-Std-Opt		0.577	0.261	1×10^{-4}	0.94	6.45
Bonny silt		0.097	0.367	0.002	0.99	14.13
Hopi silt		0.158	0.122	0.022	0.82	13.23
Iowa silt		0.121	0.148	0.014	0.96	10.59
Claystone		0.266	0.348	7.4×10^{-4}	0.87	90.86
Bentonite		0.356	0.183	0.023	0.98	1.86
Missouri clay		0.227	0.322	0.003	1.00	25.92
Sand 1	Cohesionless soils	0.148	0.643	0.980	0.98	0.10
Sand 2		0.059	2.348	0.999	0.97	0.30
Sand 3		0.089	1.745	1.045	0.98	0.29
Sand 4		0.076	1.076	0.967	0.93	0.26
Sand 5		0.055	1.255	1.010	0.86	0.31

Note: RMSE, root mean square error.

dry status is substantially greater than that of the saturated state.

5. Conclusions

A new model devoted to G_{unsat} of unsaturated soil is proposed and verified using measured data from the literature. The results show that the proposed model can well characterize the trend of SMF. Unlike previous models developed based on an empirical basis, this new model is derived through a rather rigorous theoretical analysis. The pores in unsaturated soil are divided into two groups including (i) wet pores that are saturated and (ii) dry pores that are completely dry. The modified SWCC in the form of degree of saturation is employed to relate suction to water content by incorporating the incompressible pores. Two parameters n and C within this model are determined using the least-square method. Parameter n governs the peak of the characteristic curve of G_{unsat}, while C determines the ratio between shear modulus of the soil in the saturated state and in the dry state. The fitting results revealed that the value of C is near zero for cohesive soils and one for cohesionless soils. The proposed method provides an alternative method for the estimation of the mechanical property, such as the shear modulus, of the geological material in an unsaturated condition.

Acknowledgements

The authors would like to acknowledge the financial support they received from the National Natural Science Foundation of China (Nos. 52078128, 52378328, 52178317, and 52378329) and Enterprise Development Grant (Co-Innovation Program): BZ2023016 (Jiangsu) and CIP-2207-CN1064 (Singapore).

Article information

History dates

Received: 1 August 2023
Accepted: 27 December 2023
Accepted manuscript online: 17 January 2024
Version of record online: 3 July 2024

Copyright

Data availability

No data.

Author information

Author ORCIDs

Qian Zhai https://orcid.org/0000-0003-4619-2821
Guoliang Dai https://orcid.org/0000-0002-8574-0889

Author notes

Harianto Rahardjo served as Editorial Board Member at the time of manuscript review and acceptance and did not handle peer review and editorial decisions regarding this manuscript.

Author contributions

Conceptualization: QZ, HR, WG
Data curation: RZ, AS, GD, XZ
Formal analysis: RZ
Funding acquisition: GD
Methodology: RZ, GD

Project administration: XZ
Resources: YC
Supervision: QZ
Validation: AS, WG, XZ, YC
Writing – original draft: RZ, AS, GD, WG
Writing – review & editing: QZ, HR

Competing interests

There are no competing interests.

References

Arya, L.M., and Paris, J.S. 1981. A physicoempirical model to predict the soil moisture characteristic particle-size distribution and bulk density data. Soil Science Society of America Journal, **45**: 1023–1030. doi:10.2136/sssaj1981.03615995004500060004x.

Biglari, M., Mancuso, C., d'Onofrio, A., Jafari, M.K., and Shafiee, A. 2011. Modelling the initial shear stiffness of unsaturated soils as a function of the coupled effects of the void ratio and the degree of saturation. Computers and Geotechnics, **38**(5): 709–720. doi:10.1016/j.compgeo.2011.04.007.

Bishop, A.W. 1959. The principle of effective stress. Teknisk Ukeblad, **39**: 859–863.

Burland, J. 1989. Ninth Laurits Bjerrum Memorial Lecture: "Small is beautiful"—the stiffness of soils at small strains. Canadian Geotechnical Journal, **26**(4): 499–516. doi:10.1139/t89-064.

Delage, P., Audiguier, M., Cui, Y.-J., and Howat, M.D. 1996. Microstructure of a compacted silt. Canadian Geotechnical Journal, **33**(1): 150–158. doi:10.1139/t96-030.

Dong, Y., and Lu, N. 2016. Correlation between small-strain shear modulus and suction stress in capillary regime under zero total stress conditions. Journal of Geotechnical and Geoenvironmental Engineering, **142**(11): 04016056. doi:10.1061/(ASCE)GT.1943-5606.0001531.

Fredlund, D.G., and Xing, A. 1994. Equations for the soil-water characteristic curve. Canadian Geotechnical Journal, **31**(4): 521–532. doi:10.1139/t94-061.

Han, Z., and Vanapalli, S. 2016. Stiffness and shear strength of unsaturated soils in relation to soil-water characteristic curve. Géotechnique, **66**(8): 627–647.

Hardin, B.O. 1978. The nature of stress–strain behavior for soils. *In* Paper presented at the From Volume I of Earthquake Engineering and Soil Dynamics—Proceedings of the ASCE Geotechnical Engineering Division Specialty Conference, June 19–21, 1978, Pasadena, California.

Hardin, B.O., and Black, W.L. 1968. Vibration modulus of normally consolidated clay. Journal of the Soil Mechanics and Foundations Division, **94**(2): 353–369. doi:10.1061/JSFEAQ.0001100.

Iwasaki, T., and Tatsuoka, F. 1977. Effects of grain size and grading on dynamic shear moduli of sands. Soils and Foundations, **17**(3): 19–35. doi:10.3208/sandf1972.17.3_19.

Jardine, R., Potts, D., Fourie, A., and Burland, J. 1986. Studies of the influence of non-linear stress–strain characteristics in soil–structure interaction. Géotechnique, **36**(3): 377–396. doi:10.1680/geot.1986.36.3.377.

Juang, C., and Lovell, C. 1986. Measurement of pore-size density function in sand. Transportation Research Record.

Khosravi, A., and McCartney, J.S. 2012. Impact of hydraulic hysteresis on the small-strain shear modulus of low plasticity soils. Journal of Geotechnical and Geoenvironmental Engineering, **138**(11): 1326–1333. doi:10.1061/(ASCE)GT.1943-5606.0000713.

Khosravi, A., Shahbazan, P., and Pak, A. 2018. Impact of hydraulic hysteresis on the small strain shear modulus of unsaturated sand. Soils and Foundations, **58**(2): 344–354.

Kuila, U., and Prasad, M. 2013. Specific surface area and pore-size distribution in clays and shales. Geophysical Prospecting (Rock Physics for Reservoir Exploration, Characterisation and Monitoring), **61**(2): 341–362.

Kutílek, M., Jendele, L., and Panayiotopoulos, K.P. 2006. The influence of uniaxial compression upon pore size distribution in bi-modal soils. Soil and Tillage Research, **86**(1): 27–37. doi:10.1016/j.still.2005.02.001.

Lloret, A., Villar, M.V., Sanchez, M., Gens, A., Pintado, X., and Alonso, E. 2003. Mechanical behaviour of heavily compacted bentonite under high suction changes. Géotechnique, **53**(1): 27–40. doi:10.1680/geot.2003.53.1.27.

Lu, N., and Kaya, M. 2014. Power law for elastic moduli of unsaturated soil. Journal of Geotechnical and Geoenvironmental Engineering, **140**(1): 46–56. doi:10.1061/(ASCE)GT.1943-5606.0000990.

Marinho, F., Chandler, R., and Crilly, M. 1995. Stiffness measurements on an unsaturated high plasticity clay using bender elements. *In* Paper presented at the Proceedings of the First International Conference on Unsaturated Soils/Unsat'95/Paris/France/6–8 September 1995. Vol. 2.

Minagawa, H., Nishikawa, Y., Ikeda, I., Miyazaki, K., Takahara, N., and Sakamoto, Y., 2008. Characterization of sand sediment by pore size distribution and permeability using proton nuclear magnetic resonance measurement. Journal of Geophysical Research, **113**(B7). doi:10.1029/2007JB005403.

Monroy, R., Zdravkovic, L., and Ridley, A. 2010. Evolution of microstructure in compacted London Clay during wetting and loading. Géotechnique, **60**(2): 105–119.

Ng, C.W.W., and Xu, J. 2012. Effects of current suction ratio and recent suction history on small-strain behaviour of an unsaturated soil. Canadian Geotechnical Journal, **49**(2): 226–243. doi:10.1139/t11-097.

Ng, C.W.W., and Yung, S.Y. 2008. Determination of the anisotropic shear stiffness of an unsaturated decomposed soil. Géotechnique, **58**(1): 23–35. doi:10.1680/geot.2008.58.1.23.

Ng, C.W.W., Xu, J., and Yung, S. 2009. Effects of wetting–drying and stress ratio on anisotropic stiffness of an unsaturated soil at very small strains. Canadian Geotechnical Journal, **46**(9): 1062–1076. doi:10.1139/T09-043.

Ngoc, T.P., Fatahi, B., and Khabbaz, H. 2019. Impacts of drying–wetting and loading–unloading cycles on small strain shear modulus of unsaturated soils. International Journal of Geomechanics, **19**(8): 04019090. doi:10.1061/(ASCE)GM.1943-5622.0001463.

Oh, W.T., and Vanapalli, S.K. 2014. Semi-empirical model for estimating the small-strain shear modulus of unsaturated non-plastic sandy soils. Geotechnical and Geological Engineering, **32**: 259–271. doi:10.1007/s10706-013-9708-5.

Oloo, S. 1998. The application of unsaturated soil mechanics theory to the design of pavements. *In* Paper presented at the Proceedings of the First International Conference on the Bearing Capacity of Roads and Airfields, BCRA'98.

Otálvaro, I.F., Neto, M.P.C., and Caicedo, B. 2015. Compressibility and microstructure of compacted laterites. Transportation Geotechnics, **5**: 20–34.

Picornell, M., and Nazarian, S. 1998. Effects of soil suction on the low-strain shear modulus of soils. *In* Second International Conference on Unsaturated Soils, Beijing. Vol. 2.pp. 102–107.

Qian, X., Gray, D.H., and Woods, R.D. 1993. Voids and granulometry: effects on shear modulus of unsaturated sands. Journal of Geotechnical Engineering, **119**(2): 295–314. doi:10.1061/(ASCE)0733-9410(1993)119:2(295).

Richart, F.E., Hall, J.R., and Woods, R.D. 1970. Vibrations of soils and foundations.

Romero, E., and Simms, P.H. 2008. Microstructure investigation in unsaturated soils: a review with special attention to contribution of mercury intrusion porosimetry and environmental scanning electron microscopy. Geotechnical and Geological Engineering, **26**: 705–727. doi:10.1007/s10706-008-9204-5.

Satyanaga, A., Rahardjo, H., and Zhai, Q. 2017. Estimation of unimodal water characteristic curve for gap-graded soil. Soils and Foundations, **57**: 789–801. doi:10.1016/j.sandf.2017.08.009.

Sawangsuriya, A. 2006. Stiffness–suction–moisture relationship for compacted soils. Ph.D. The University of Wisconsin—Madison, Wisconsin, United States.

Sawangsuriya, A., Edil, T.B., and Bosscher, P.J. 2009. Modulus–suction–moisture relationship for compacted soils in postcompaction state. Journal of Geotechnical and Geoenvironmental Engineering, **135**(10): 1390–1403. doi:10.1061/(ASCE)GT.1943-5606.0000108.

Shibata, T., and Soelarno, D.S. 1975. Stress–strain characteristics of sands under cyclic loading. *In* Paper presented at the Proceedings of the Japan Society of Civil Engineers.

Shibuya, S., and Tanaka, H. 1996. Estimate of elastic shear modulus in Holocene soil deposits. Soils and Foundations, **36**(4): 45–55. doi:10.3208/sandf.36.4_45.

Stingaciu, L., Weihermüller, L., Haber-Pohlmeier, S., Stapf, S., Vereecken, H., and Pohlmeier, A. 2010. Determination of pore size distribution and hydraulic properties using nuclear magnetic resonance relaxometry: a comparative study of laboratory methods. Water Resources Research, **46**(11). doi:10.1029/2009WR008686. PMID: 24604925.

Suprunenko, G. 2015. Suction-controlled cyclic triaxial test to measure strain-dependent dynamic shear modulus of unsaturated sand. M.S. University of New Hampshire, New Hampshire, United States.

Vanapalli, S., Fredlund, D., Pufahl, D.E., and Clifton, A.W. 1996. Model for the prediction of shear strength with respect to soil suction. Canadian Geotechnical Journal **33**: 379–392.

Wang, M., Chen, P., Yi, P., and Ma, T. 2023. Effect of fines content on pore distribution of sand/clay composite soil. Sustainability, **15**(12): 9216. doi:10.3390/su15129216.

Witczak, M., Pellinen, T., and El-Basyouny, M. 2002. Pursuit of the simple performance test for asphalt concrete fracture/cracking. Journal of the Association of Asphalt Paving Technologists, 71.

Wu, S., Gray, D.H., and Richart, F., Jr. 1984. Capillary effects on dynamic modulus of sands and silts. Journal of Geotechnical Engineering, **110**(9): 1188–1203.

Zhai, Q., and Rahardjo, H. 2012. Determination of soil-water characteristic curve variables. Computers and Geotechnics, **42**: 37–43. doi:10.1016/j.compgeo.2011.11.010.

Zhai, Q., and Rahardjo, H. 2015. Estimation of permeability function from the soil-water characteristic curve. Engineering Geology, **199**: 148–156. doi:10.1016/j.enggeo.2015.11.001.

Zhai, Q., Rahardjo, H., and Satyanaga, A. 2017. Effects of residual suction and residual water content on the estimation of permeability function. Geoderma, **303**: 165–177. doi:10.1016/j.geoderma.2017.05.019.

Zhai, Q., Rahardjo, H., Satyanaga, A., and Dai, G.L. 2019. Estimation of unsaturated shear strength from soil-water characteristic curve. Acta Geotechnica, **14**(6): 1977–1990. doi:10.1007/s11440-019-00785-y.

Zhai, Q., Rahardjo, H., Satyanaga, A., and Dai, G.L. 2020a. Estimation of the soil-water characteristic curve from the grain size distribution of coarse-grained soils. Engineering Geology, **267**: 105502. doi:10.1016/j.enggeo.2020.105502.

Zhai, Q., Rahardjo, H., Satyanaga, A., and Dai, G.L. 2020b. Estimation of tensile strength of sandy soil from soil-water characteristic curve. Acta Geotechnica, **15**: 3371–3381. doi:10.1007/s11440-020-01013-8.

Zhou, C. 2014. Experimental study and constitutive modelling of cyclic behaviour at small strains of unsaturated silt at various temperatures. Ph.D. Hong Kong University of Science and Technology, Hong Kong.